Orthorhombic Jahn-Teller distortion and Si-OH in mozartite, $CaMn^{3+}O[SiO_3OH]$: A single-crystal X-ray, FTIR, and structure modeling study

Daniel Nyfeler,[1] Christina Hoffmann,[1] Thomas Armbruster,[1] Martin Kunz,[2] and Eugen Libowitzky[3]

[1]Laboratorium für chemische und mineralogische Kristallographie, Universität Bern, Freiestrasse 3, CH-3012 Bern, Switzerland
[2]High Pressure Group, European Synchrotron Radiation Facility, BP 220, Avenue des Martyrs, F-38043 Grenoble, Cedex, France
[3]Institut für Mineralogie und Kristallographie, Universität Wien-Geozentrum, Althanstrasse 14, A-1090 Wien, Austria

Abstract

The structure of mozartite, $CaMn^{3+}O[SiO_3OH]$, was refined in space group $P2_12_12_1$ from X-ray single-crystal data collected at 100 K ($R = 2.45\%$, $R_w = 2.62\%$), 300 K ($R = 2.60\%$, $R_w = 2.68\%$), and 500 K ($R = 2.79\%$, $R_w = 2.81\%$). The $Mn^{3+}O_6$ octahedron shows approximately orthorhombic geometry, which is explained by a combination of a tetragonally compressed Jahn-Teller effect with lattice-induced stress. Comparison with isostructural vuagnatite, $CaAl(OH)SiO_4$, which shows no distortions due to electronic effects, indicates that the distorted octahedral geometry in mozartite causes shifts in valence sums of the O atoms that are hydrogen bonded. As a result, the OH group in mozartite is located at the isolated SiO_4 apex and is not linked to the octahedron as reported for isostructural minerals. Isostructural minerals of the adelite group with tetrahedral As^{5+} and V^{5+} exhibit a different Jahn-Teller distortion with tetragonally elongated geometry for octahedral $Cu^{2+}O_6$.

The $O\text{-}H \cdots O$ distance of <2.5 Å in mozartite is one of the shortest hydrogen bonded $O \cdots O$ distances in minerals and leads to a diffuse FTIR absorption peak (stretching mode) polarized parallel to b between 1300 and 1700 cm^{-1}.

Introduction

The structure of mozartite, $CaMn^{3+}O[SiO_3OH]$, was first studied by Basso et al. (1993) using crystals from the Cerchiara mine, Northern Apennines, Italy. Mozartite is isostructural with vuagnatite, $CaAl(OH)SiO_4$, (McNear et al. 1976) and four members of the adelite group: vanadate calciovolborthite, $CaCu(OH)VO_4$ (Basso et al. 1989); arsenates austinite, $CaZn(OH)AsO_4$ (Giuseppetti and Tadini 1988); conichalcite, $CaCu(OH)AsO_4$ (Qurashi and Barnes 1963); and nickelaustinite, $Ca(Ni,Zn)(OH)AsO_4$ (Cesbron et al. 1987). These minerals, with the general formula $CaM(OH)TO_4$, crystallize in the acentric space group $P2_12_12_1$. The structure has the characteristic motif referred to as "backbone" (Shen and Moore 1982), consisting of a linear chain of edge-sharing octahedra with attached single tetrahedra (Gottardi 1967) developed along a twofold screw axis (Fig. 1).

The silicates mozartite and vuagnatite differ from the arsenates and vanadate of the adelite group by their charge distribution. In vuagnatite and mozartite the edge-sharing octahedral chains are formed by trivalent cations (Al, Mn^{3+}), whereas in the adelite group divalent cations (Cu, Ni, Zn) form the chains. The deficit of positive charges is stoichiometricly balanced by the valence of the tetrahedral cations (As^{5+}, V^{5+}) in the minerals of the adelite group, whereas tetrahedral Si^{4+} occurs in vuagnatite and mozartite. In the adelite group of minerals, this higher valence state of the tetrahedral cation leads to electrostatically more saturated O atoms forming the tetrahedron and their affinity for protonization becomes negligible. The divalent octahedral cation, on the other hand, yields a formal undersaturation of one of its next O atoms, favoring the formation of an OH group.

Our attention was focused on mozartite when we detected unreasonable valence sums for O atoms coordinating Si and Mn (Basso et al. 1993). The original geometry described by Basso et al. (1993) is characterized by the distances O5-H = 1.05 Å and H $\cdots$ O2 = 1.45 Å. The O5 atom connects two $Mn^{3+}O_6$ octahedra and bonds to one Ca atom. Another O atom, O2, is part of a SiO_4 tetrahedron and bonds to two Ca atoms. This arrangement, according to the bond valence concept of Brown and Altermatt (1985), results in the following valence sums (excluding H): 1.376 valence units (v.u.) for O2 and 1.878 for O5. This suggests that the OH group is at O2 rather than at O5 as hitherto assumed.

In addition to the proton position, the Jahn-Teller distortion of the $Mn^{3+}O_6$ octahedron is discussed in this paper. To elucidate the influence of lattice stress on the orientation of the Jahn-Teller distortion, network calculations were performed. Single-crystal X-ray data were collected at three temperatures (100, 300, and 500 K) to test the temperature dependence of the Jahn-Teller distortion. The short hydrogen bonded $O\text{-}H \cdots O$ distance of <2.50 Å initiated an IR spectroscopic investigation.
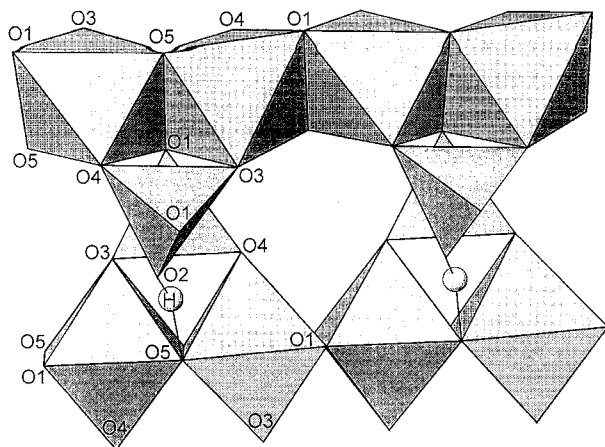
FIGURE 1. Simplified representation (*a-c* plane) of the mozartite structure, composed of linear chains of edge-sharing octahedra with attached single tetrahedra developed along a twofold screw axis. SiO_4 and MnO_6 are shown as polyhedra.

EXPERIMENTAL METHOD

Sample description and single-crystal X-ray data collection

Mozartite crystals from the N'chwaning mine, Kalahari manganese field, Republic of South Africa, have the composition $Ca_{0.944}(Mn_{0.963}Fe_{0.027}Mg_{0.011})Si_{0.969}O_4(OH)$ (Jens Gutzmer, electron microprobe analysis, personal communication). At this locality, mozartite is associated with andradite and hausmannite (the latter intergrown with a fibrous serpentine phase) grown on calcite and barite. The euhedral, red-brown crystals average 0.2 mm in diameter. Twinning or intergrowth is common, thus a careful search for a suitable single crystal was required.

A single crystal 150 × 175 × 125 μm³ in dimension was used for the acquisition of the X-ray diffraction data. The crystal was mounted on a silica-glass needle using a high-temperature resistant epoxy resin, and the same crystal was used for the collection of three data sets at 100, 300, and 500 K. X-ray intensities were measured on a CAD4 single-crystal diffractometer with graphite-monochromatized MoKα radiation up to θ = 40° using the 1.5° ω + 0.3tan θ scan mode.

During the data collection at 500 K the crystal was heated by a regulated (±5 K) hot-air blower. For the measurement at 100 K, a conventional liquid nitrogen cooling device with an accuracy of ±2 K was used. At each temperature, 12 reflections were used to determine the cell parameters.

An empirical absorption correction was applied using the Ψ-scan method for selected reflections. Data reduction, including background, Lorentz, and polarization corrections, was performed with the SDP program system (Enraf-Nonius 1983). The program SHELXTL (Siemens 1990) was used to solve and refine the structure. Scattering factors for neutral atoms were used. Atomic positions were refined using >1100 reflections with $I > 3\sigma_I$ for all

three data sets. The positions of all atoms except H were refined using initially isotropic, then anisotropic, displacement parameters (ADP). After refinement of all Mn, Ca, and O atoms, difference-Fourier maps showed a diffuse positive electron-density cloud between O2 and O5, indicating the presence of an H atom. This H position was restrained to have a 1.25 Å distance to both neighboring O atoms with a weight factor of 0.1. Nevertheless, a subsequent refinement yielded a proton position close to O2 hydrogen bonded to O5. In the final refinements the O2-H bond was restrained to 0.95 Å with a weight factor of 0.03, allowing the H atom position to be determined accurately. The reflections were weighted as $1/[\sigma_F^2 + gF^2]$, where g was fixed at 0.0001. Observed and calculated structure factors are given in Table 1[1]. Bond valences were calculated using the parameters recommended by Brese and O'Keeffe (1991).

FTIR spectroscopy

The spectra were measured on a Nicolet 60SX FTIR spectrometer using a glowbar light source, a KBr beam splitter, and a liquid-nitrogen cooled MCT detector. For the low-temperature spectra (84 ± 2 K) a commercial cryo-cell (MMR Technologies) with KBr windows was used. Polarized single-crystal spectra were measured using a gold wire grid polarizer on an AgBr substrate and an elliptical sample aperture of 150 × 130 μm². The doubly polished mozartite crystal applied for the measurement was 150 × 130 μm² wide and 6(±1) μm thick. A detailed description of the preparation of the small crystal plate for FTIR spectroscopy is given in an Appendix[1].

Network calculations

Bond-valence network calculations [program STRU-MO (Brown 1992)] were performed to analyze the influence of the crystal structure on the orientation of the Jahn-Teller distortion. Octahedral Mn^{3+} possesses $3d^4$ high-spin configuration, which causes (without the influence of an external force field) either an elongated or compressed tetragonal Jahn-Teller distortion. In the bond valence model, a crystal structure is viewed as a network of atoms in which cations are bonded to anions and vice versa. Analogous to the atomic valence (v_i) characterizing atoms, bond valences (v_{ij}) are defined to characterize the chemical bonds. The ideal bond valence is uniquely defined for any given structural topology by two network equations (Brown 1989; Brown 1992):

$$V_i = \text{sum}(j)\ v_{ij}\ \text{(bond valence sum rule)} \quad (1)$$

$$\text{sum(loop)}\ v_{ij} = 0\ \text{(equal valence rule)} \quad (2)$$

In addition, bond valences are uniquely linked to bond

TABLE 2. Cell parameters (Å), number of reflections, and R values of mozartite ($P2_12_12_1$) at 100, 300, and 500 K

	a	b	c	V	Reflections ($I > 3\sigma_I$)	Parameters	R (%)	R_w (%)
100 K	5.837(1)	7.211(1)	8.693(1)	365.89	1537	71	2.45	2.62
300 K	5.842(1)	7.228(1)	8.704(1)	367.53	1376	71	2.60	2.68
500 K	5.846(1)	7.248(1)	8.726(1)	369.74	1189	71	2.79	2.81
Δ	0.009	0.037	0.033					

Note: Δ represents the difference of cell parameters between 500 and 100 K.
$R = (\Sigma|F_{obs} - F_{calc}|)/(\Sigma F_{obs})$
$R_w = \{[\Sigma(\text{weight}|F_{obs} - F_{calc}|)^2]/[\Sigma(\text{weight}\cdot F_{obs}^2)]\}^{1/2}$

lengths for any given cation-anion pair by the empirically derived relationship:

$$\text{sum}(j)\ v_{ij} = \text{sum}(j)\ \exp[(R_{ij} - d_{ij})/0.37] \qquad (3)$$

where d_{ij} are the actual bond lengths and R_{ij} are cation-anion pair-specific constants tabulated by Brown and Altermatt (1985) and Breese and O'Keeffe (1991). The concept of the bond-valence model is that each atom tends to distribute its valence as equally as possible among the bonds that it forms. The application of Equations 1–3 to a given bond topology allows the comparison between ideal bond lengths predicted for a crystal structure free of steric and electronic distortions on one hand and the actual observed bond lengths on the other hand. Because the bond-valence model does not take into account steric and electronic distortions, it serves as a useful tool for finding and characterizing such effects (Kunz and Brown 1995). In addition, such effects can also be incorporated into the network equations by applying empirically derived weights to the bond valences:

$$v_{ij} = V_{ij} / c_{ij} \qquad (4)$$

where V_{ij} is the observed value and c_{ij} corresponds to the weight applied to a particular bond. By this procedure a weight <1 weakens a bond and thus tends to lengthen it, whereas $c_{ij} > 1$ strengthens and therefore shortens a bond.

Valence weights (Kunz and Brown 1995) of 0.6 and 5.0 for H $\cdots$ O5 and H-O2, respectively, were chosen to give an optimal bond length modeling of the O-H $\cdots$ O environment. Weighting O-H bonds in the network calculations is essential, since the equal-valence rule forces the O-H $\cdots$ O bonds to be equal, therefore not taking into account the intrinsic asymmetry of O-H $\cdots$ O configurations (Brown 1976; 1992). In addition, a calculation was performed with weights according to the O5-H $\cdots$ O2 arrangement suggested by Basso et al. (1993). Furthermore, a valence-least-squares refinement was performed to obtain an estimate of H coordinates. This method is equivalent to a distance-least-squares refinement (Baerlocher et al. 1977) except that valences are used as the target values instead of bond lengths. In this refinement only H coordinates were varied and the network-derived bond valences were used as target valences.

RESULTS

Cell parameters (and their difference from 100 to 500 K), number of reflections, and R values from XRD for

all three temperatures investigated are given in Table 2. The thermal expansion is more pronounced for b and c than for a. Atomic coordinates and displacement parameters are given in Table 3, cation-oxygen distances are shown in Table 4. Of the anisotropically refined atoms, the O2 atom has the highest and most strongly anisotropic displacement parameters. In Table 5 the ADP contributions parallel (par) and perpendicular (perp) to the Si-O bonds are distinguished, providing insight into the nature of the disorder of the tetrahedron. Two additional empirical values are calculated:

$$\Delta U(\text{par}) = U2(\text{par}) - U1(\text{par}) \qquad (5)$$

$$\Delta U(\text{perp}) = U2(\text{perp}) - U1(\text{perp}) \qquad (6)$$

where $U2$ and $U1$ are the respective mean-square displacement amplitudes of O toward Si and of Si toward O. The differences of mean-square displacement amplitudes reflect the rigidity of the tetrahedron (Bartelmehs et al. 1995; Dunitz et al. 1988; Kunz and Armbruster 1990). Furthermore, the average values for $\Delta U(\text{par})$ and $\Delta U(\text{perp})$, the latter excluding the values for O2, distinguish differences in the nature of librational motion of O2 (H-bearing) and the remaining Si-coordinating O atoms. In Figure 2, these average ΔU values are plotted vs. temperature. The $\Delta U(\text{par})$ remains constant as a function of temperature; $\Delta U(\text{perp})$, however, increases. With increasing temperature O2 shows both the highest $U2(\text{perp})$ and the highest $\Delta U(\text{perp})$. Bond valences and valence sums, excluding H, are shown in Table 6[1]. All cations and anions yield satisfying valence sums, except that O2 has a lower value than the other O atoms. The average Ca-O distance of the eightfold-coordinated Ca increases from 2.478 Å at 100 K to 2.491 Å at 500 K. A slight increase was also observed for the $Mn^{3+}O_6$ octahedron, when the average Mn-O distance increases from 2.017 Å at 100 K to 2.023 Å at 500 K. The short Mn-O5 bonds do not increase with temperature. Within this temperature range the Si-O distances remain unchanged.

For the localization of H, the procedure described in the experimental section yielded physically reasonable bond distances and angles. The resulting O2-H, H $\cdots$ O5, and O2 $\cdots$ O5 distances are given in Table 4. The data generated from the two network calculations are listed in Table 6. Using network-derived valences from the O2-H $\cdots$ O5 model a valence least-squares refinement converged at a H position (cited H_{calc} in Table 3) 0.98 Å from O2 and 1.507 Å from O5, which agrees within three

TABLE 3. Atomic coordinates, anisotropic displacement parameters, and U_{eq} values for mozartite at 100, 300, and 500 K

	x/a	y/b	z/c	U_{11}	U_{22}	U_{33}	U_{12}	U_{13}	U_{23}	U_{eq}
						100 K				
Ca	0.02238(8)	0.37501(7)	0.67430(5)	0.0040(2)	0.0035(2)	0.0034(2)	0.0001(1)	0.0002(2)	0.0008(1)	0.00360(9)
Mn	0.74729(8)	0.25758(5)	0.99647(4)	0.00218(9)	0.00282(9)	0.0030(1)	−0.00030(8)	0.0004(2)	−0.0001(1)	0.00266(5)
Si	0.5104(1)	0.63076(9)	0.81680(7)	0.0023(3)	0.0027(2)	0.0026(3)	−0.0006(2)	−0.0002(2)	0.0005(2)	0.0025(1)
O1	0.4894(3)	0.4536(2)	0.9338(2)	0.0033(6)	0.0040(6)	0.0038(6)	0.0005(6)	0.0002(6)	0.0001(4)	0.0037(3)
O2	0.0741(3)	0.7006(2)	0.0619(2)	0.0061(7)	0.0034(6)	0.0051(7)	−0.0002(5)	−0.0009(5)	−0.0015(5)	0.0049(4)
O3	0.2708(3)	0.6578(2)	0.7220(2)	0.0025(6)	0.0042(6)	0.0034(6)	0.0008(5)	−0.0002(5)	0.0008(5)	0.0034(4)
O4	0.7379(3)	0.6217(2)	0.7067(2)	0.0036(5)	0.0056(6)	0.0034(6)	0.0011(6)	0.0001(5)	0.0006(5)	0.0042(3)
O5	0.0032(3)	0.3951(2)	0.9398(2)	0.0031(6)	0.0038(6)	0.0047(6)	−0.0004(6)	−0.0008(6)	0.0003(5)	0.0039(3)
H	0.030(7)	0.583(4)	0.033(5)							0.04(1)
						300 K				
Ca	0.0219(1)	0.37462(8)	0.67420(6)	0.0090(2)	0.0072(2)	0.0059(2)	0.0006(2)	0.0000(2)	0.0016(2)	0.0073(1)
Mn	0.7473(1)	0.25740(6)	0.99658(6)	0.0040(1)	0.0059(1)	0.0049(1)	−0.0003(1)	0.0001(2)	−0.0004(2)	0.00494(6)
Si	0.5102(1)	0.6301(1)	0.81659(8)	0.0037(3)	0.0054(3)	0.0050(3)	0.0003(3)	0.0000(3)	0.0000(3)	0.0047(2)
O1	0.4898(4)	0.4535(2)	0.9332(2)	0.0064(7)	0.0070(7)	0.0066(7)	0.0003(8)	0.0005(8)	0.0006(5)	0.0067(4)
O2	0.0716(4)	0.7020(3)	0.0624(3)	0.013(1)	0.0061(7)	0.0092(9)	−0.0004(7)	0.0010(7)	−0.0018(7)	0.0095(5)
O3	0.2714(3)	0.6573(3)	0.7222(2)	0.0045(8)	0.0076(7)	0.007(8)	0.0004(6)	−0.0003(7)	0.0019(6)	0.0065(5)
O4	0.7373(3)	0.6223(3)	0.7068(2)	0.0057(7)	0.0089(8)	0.0063(7)	0.0020(8)	0.0007(7)	0.0008(6)	0.0070(4)
O5	0.0028(3)	0.3944(2)	0.9391(2)	0.0042(6)	0.0058(7)	0.0067(7)	0.0004(8)	−0.0012(7)	0.0014(5)	0.0055(4)
H	0.03(1)	0.583(5)	0.042(6)							0.07(2)
H_{calc}	0.041	0.573	0.027							
						500 K				
Ca	0.0210(2)	0.3746(1)	0.67425(8)	0.0156(4)	0.0125(3)	0.0085(3)	0.0008(3)	0.0004(3)	0.0019(3)	0.0122(2)
Mn	0.7477(2)	0.25699(8)	0.99658(6)	0.0058(1)	0.0083(1)	0.0059(1)	−0.0005(1)	0.0007(3)	−0.0004(2)	0.00668(8)
Si	0.5096(2)	0.6290(1)	0.8163(1)	0.0072(4)	0.0082(4)	0.0069(4)	−0.0006(4)	0.0002(5)	0.0006(4)	0.0074(2)
O1	0.4907(5)	0.4531(3)	0.9333(3)	0.0106(9)	0.0095(9)	0.0096(9)	0.001(1)	0.001(1)	0.0017(6)	0.0099(5)
O2	0.0676(6)	0.7026(4)	0.0627(3)	0.023(1)	0.010(1)	0.013(1)	0.0002(9)	0.001(1)	−0.0047(9)	0.0153(7)
O3	0.2721(5)	0.6552(4)	0.7219(3)	0.005(1)	0.016(1)	0.011(1)	0.0008(8)	−0.0015(9)	0.0009(9)	0.0105(6)
O4	0.7368(5)	0.6221(4)	0.7072(3)	0.012(1)	0.015(1)	0.007(1)	0.003(1)	0.0010(9)	0.0014(9)	0.0114(6)
O5	0.0027(5)	0.3933(3)	0.9390(2)	0.0071(8)	0.0089(8)	0.010(1)	−0.001(1)	−0.002(1)	0.0005(7)	0.0087(5)
H	0.06(1)	0.579(5)	0.031(7)							0.08(3)

esd with the H position extracted from our X-ray data sets [0.91(4) Å from O2 and 1.64(4) Å from O5, for 100 K]. Polarized single-crystal FTIR spectra at 84 and 298 K are given in Figure 3.

TABLE 4. Cation-oxygen distances (Å) for mozartite at 100, 300, and 500 K

Cation	Oxygen	100 K	300 K	500 K
Ca	O1	2.430(2)	2.439(2)	2.446(2)
Ca	O2	2.608(2)	2.626(2)	2.654(3)
Ca	O2	2.473(2)	2.469(2)	2.469(3)
Ca	O3	2.489(2)	2.493(2)	2.507(3)
Ca	O3	2.537(2)	2.544(2)	2.543(3)
Ca	O4	2.449(2)	2.460(2)	2.462(3)
Ca	O4	2.523(2)	2.526(2)	2.534(3)
Ca	O5	2.316(2)	2.313(2)	2.316(2)
	Average	2.478	2.484	2.491
Mn	O1b	2.135(2)	2.139(2)	2.141(3)
Mn	O1d	2.164(2)	2.169(2)	2.171(3)
Mn	O3e	2.034(2)	2.040(2)	2.047(3)
Mn	O4b	2.026(2)	2.028(2)	2.038(3)
Mn	O5	1.859(2)	1.860(2)	1.858(3)
Mn	O5d	1.884(2)	1.886(2)	1.885(3)
	Average	2.017	2.020	2.023
Si	O1	1.638(2)	1.635(2)	1.637(2)
Si	O2	1.652(2)	1.647(2)	1.650(3)
Si	O3	1.634(2)	1.631(2)	1.625(3)
Si	O4	1.639(2)	1.636(2)	1.635(3)
	Average	1.641	1.637	1.637
H	O2	0.92(3)	0.91(4)	0.94(4)
H	O5	1.59(3)	1.64(4)	1.60(4)
O2	O5	2.480(2)	2.501(3)	2.517(3)

DISCUSSION

Orthorhombic distortion of the octahedron

The stereochemistry of the sixfold-coordinated Mn^{3+} complex is dominated by Jahn-Teller vibronic coupling. The resulting distortion produces either a tetragonally elongated or compressed octahedron with quite different electronic ground states (Hitchman 1994).

The $Mn^{3+}O_6$ octahedron in mozartite shows distorted Mn-O distances (Table 4), but at a first glance it is not obvious whether an elongated or a compressed Jahn-Teller distortion exists. The O1-M-O1 octahedral diagonal is elongated (4.308 Å at room temperature), O5-M-O5 is compressed (3.746 Å), and O3-M-O4 is intermediate (4.068 Å). One could argue that such an unusual distortion is caused by static or dynamic disorder of differently oriented, tetragonally compressed and elongated directions. However, such a disorder should lead to substantial electronic "smearing" evaluated in terms of ΔU (Table 5) along the Mn-O bonding vector. Assuming disorder of a short Mn-O distance of 1.8 Å with a long Mn-O distance of 2.2 Å would yield a mean-square difference distance of 0.04 Å² (Chandrasekhar and Bürgi 1984), which is on the order of one magnitude higher than the observed average ΔU values of about 0.001–0.004 Å². These ΔU values are in good agreement with those for octahedral Fe^{3+} ($\Delta U = 0.001$ Å²) in andradite (Armbruster and Geiger 1993) thus ruling out Jahn-Teller disorder. However, the observed orthorhombic geometry of the MnO_6 poly-

TABLE 5. Mean-square vibrational amplitudes parallel and perpendicular to the Si-O and Mn-O bond vectors

1	2	$U1$(par)	$U2$(par)	$U1$(perp)	$U2$(perp)	ΔU(par)	ΔU(perp)
				100 K			
Si	O1	0.0021(2)	0.0037(6)	0.0027(2)	0.0036(6)	0.0016(6)	0.0009(6)
Si	O2	0.0029(2)	0.0034(6)	0.0023(2)	0.0055(6)	0.0005(6)	0.0032(6)
Si	O3	0.0023(2)	0.0024(6)	0.0026(2)	0.0038(6)	0.0001(6)	0.0012(6)
Si	O4	0.0025(2)	0.0034(6)	0.0025(2)	0.0046(6)	0.0009(6)	0.0021(6)
Average						0.0008(3)	⟨0.0014(3)⟩
Mn	O1	0.0030(1)	0.0031(6)	0.0025(1)	0.0040(6)	0.0001(6)	0.0015(6)
Mn	O1	0.0030(1)	0.0041(6)	0.0025(1)	0.0035(6)	0.0011(6)	0.0010(6)
Mn	O3	0.0029(1)	0.0029(6)	0.0025(1)	0.0036(6)	0.0000(6)	0.0011(6)
Mn	O4	0.0029(1)	0.0034(6)	0.0025(1)	0.0046(6)	0.0005(6)	0.0021(6)
Mn	O5	0.0020(1)	0.0034(6)	0.0030(1)	0.0041(6)	0.0014(6)	0.0011(6)
Mn	O5	0.0020(1)	0.0034(6)	0.0030(1)	0.0041(6)	0.0014(6)	0.0011(6)
Average						⟨0.0008(2)⟩	⟨0.0013(2)⟩
				300 K			
Si	O1	0.0053(3)	0.0061(7)	0.0044(3)	0.0069(7)	0.0008(8)	0.0025(8)
Si	O2	0.0053(3)	0.0059(7)	0.0044(3)	0.0110(7)	0.0006(8)	0.0066(8)
Si	O3	0.0040(3)	0.0049(8)	0.0051(3)	0.0074(8)	0.0009(9)	0.0023(9)
Si	O4	0.0041(3)	0.0049(7)	0.0051(3)	0.0079(7)	0.0008(8)	0.0028(8)
Average						⟨0.0008(4)⟩	⟨0.0025(4)⟩
Mn	O1	0.0055(1)	0.0066(7)	0.0046(1)	0.0067(7)	0.0011(8)	0.0021(8)
Mn	O1	0.0053(1)	0.0064(7)	0.0048(1)	0.0069(7)	0.0011(8)	0.0021(8)
Mn	O3	0.0048(1)	0.0062(8)	0.0050(1)	0.0067(8)	0.0014(9)	0.0017(9)
Mn	O4	0.0048(1)	0.0062(7)	0.0050(1)	0.0074(7)	0.0014(8)	0.0024(8)
Mn	O5	0.0045(1)	0.0036(7)	0.0052(1)	0.0066(7)	−0.0009(8)	0.0014(8)
Mn	O5	0.0044(1)	0.0053(7)	0.0052(1)	0.0056(7)	0.0009(8)	0.0004(8)
Average						⟨0.0008(3)⟩	⟨0.0019(3)⟩
				500 K			
Si	O1	0.0071(4)	0.0081(9)	0.0076(4)	0.0110(9)	0.0010(10)	0.0034(10)
Si	O2	0.0079(4)	0.0071(11)	0.0071(4)	0.0190(11)	−0.0008(12)	0.0119(12)
Si	O3	0.0072(4)	0.0058(10)	0.0076(4)	0.0132(10)	−0.0014(11)	0.0056(11)
Si	O4	0.0071(4)	0.0088(10)	0.0076(4)	0.0125(10)	0.0017(11)	0.0049(11)
Average						⟨0.0005(6)⟩	⟨0.0046(6)⟩
Mn	O1	0.0077(1)	0.0092(9)	0.0061(1)	0.0102(9)	0.0015(9)	0.0041(9)
Mn	O1	0.0079(1)	0.0096(9)	0.0061(1)	0.0100(9)	0.0017(9)	0.0039(9)
Mn	O3	0.0061(1)	0.0104(10)	0.0071(1)	0.0106(10)	0.0043(10)	0.0035(10)
Mn	O4	0.0061(1)	0.0077(10)	0.0071(1)	0.0132(10)	0.0016(10)	0.0061(10)
Mn	O5	0.0059(1)	0.0076(8)	0.0071(1)	0.0092(8)	0.0017(8)	0.0021(8)
Mn	O5	0.0061(1)	0.0079(8)	0.0071(1)	0.0090(8)	0.0018(8)	0.0019(8)
Average						⟨0.0021(4)⟩	⟨0.0036(4)⟩

Note: O2 was excluded from the calculation of the average (see text for explanation). $\Delta U = U2 - U1$ (Å^2).

hedron is not unusual in crystals and well described for sixfold-coordinated Cu^{2+} with similar electronic properties as Mn^{3+} (Gazo et al. 1976; Hitchman 1994; Riley et al. 1987). The latter authors state that the Jahn-Teller active vibration is doubly degenerate, and transition between the two tetragonal geometries (compressed and elongated) can occur by overcoming only small energy barriers (Hitchman 1994). Lattice forces are able to stabilize intermediate states such as the orthorhombic coordination geometry of $Cu^{2+}O_6$ and $Mn^{3+}O_6$ polyhedra.

The lattice-induced stress in mozartite is caused by mainly two interactions, namely cation-cation repulsion and electrostatic interactions imposed by valence sum requirements. The M^{3+}-M^{3+} repulsion in mozartite stretches the O1-M-O1 distance to a greater extent than in isostructural vuagnatite, where Al^{3+} with a smaller ionic radius occupies the M site. This allows a shorter Al-Al distance of 2.847 Å (McNear et al. 1976), whereas in mozartite Mn^{3+} repulses its next Mn^{3+} neighbor to a distance of 2.924 Å (at room temperature), yielding a long O1-M-O1 diagonal. In spite of this long O1-M-O1 distance in mozartite, O1 has the highest valence sums of all O atoms,

indicating that a shortening of these bonds is not favorable. The octahedral diagonals in vuagnatite (O1-M-O1 3.997 Å; O3-M-O4 3.848 Å; O5-M-O5 3.680 Å) predetermine the orthorhombic geometry observed in an enhanced fashion in mozartite. This observation is an example where the orientation of the electronic effect (Jahn-Teller) follows and enhances the topologically induced distortion (Kunz and Brown 1995; Hoffmann et al. 1997). Comparison between the Al octahedron in vuagnatite and the Mn^{3+} octahedron in mozartite indicates that in spite of the larger diameter (Shannon 1976) of Mn^{3+} (1.29 Å) relative to Al (1.07 Å), only the diagonals O1-M-O1 and O3-M-O4 adapt to the larger Mn^{3+} size in mozartite (increases of 0.311 and 0.213 Å, respectively). The diagonal O5-M-O5 for Mn^{3+} is only 0.066 Å longer than the corresponding value for Al. This observation indicates that the orthorhombic distortion of Mn^{3+} is a combination of a tetragonally compressed Jahn-Teller effect and lattice-induced stress.

A similar enhancing effect was observed in the isostructural vanadate and arsenates. Both austinite, $CaZn(OH)AsO_4$ (Giuseppetti and Tadini 1988), and nick-

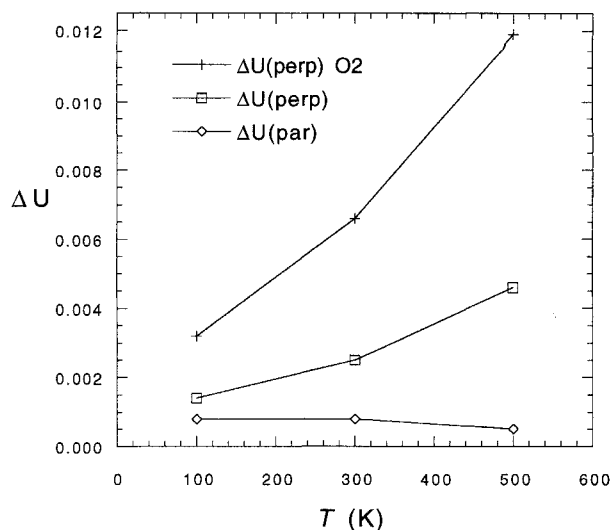**FIGURE 2.** The ΔU values of the tetrahedral O atoms parallel and perpendicular to the Si-O bonds vs. temperature, reflecting the rigid-body motion of the tetrahedron. ΔU(perp) of O2 is shown separately to point out the additional libration of the OH group.

FIGURE 3. Polarized single-crystal FTIR spectra of mozartite at 298 and 84 K.

elaustinite, $Ca(Ni,Zn)(OH)AsO_4$ (Cesbron et al. 1987), with octahedral Ni and Zn (not subject to electronic distortion), have distorted octahedra, with diagonals of 4.331 Å (O1-M-O1), 4.417 Å (O3-M-O4), and 3.877 Å (O5-M-O5) for austinite and 4.30 Å (O1-M-O1), 4.29 Å (O3-M-O4), and 3.93 (O5-M-O5) for nickelaustinite. Conichalcite, $CaCu(OH)AsO_4$ (Qurashi and Barnes 1963), and calciovolborthite, $CaCu(OH)VO4$ (Basso et al. 1989), contain Cu^{2+}, which is subject to a Jahn-Teller distortion. Ionic radii of octahedral Cu^{2+} (0.73 Å), Ni (0.69 Å), and Zn (0.74 Å) are very similar (Shannon 1976). The enhanced distortion for Cu^{2+} results in octahedral diagonals of 4.13 Å (O1-M-O1), 4.66 Å (O3-M-O4), and 3.90 Å (O5-M-O5) for conichalcite and 4.127 Å (O1-M-O1), 4.752 Å (O3-M-O4), and 3.815 Å (O5-M-O5) for calciovolborthite. The electronic effect lengthens the long O3-M-O4 diagonal and shortens the intermediate O1-M-O1 octahedral axis, whereas the O5-M-O5 axis remains short. Thus the observed geometry for the $Cu^{2+}O_6$ octahedron is close to a tetragonally elongated distortion. The relatively short O5-M-O5 diagonal indicates a restricted spatial flexibility along the octahedral chains, parallel to a, caused by the tetrahedra linking the octahedral O5 apices, as shown in Figure 1. This is also confirmed by the temperature behavior of mozartite, where a (approximately parallel to O5-M-O5) increases only slightly (0.009 Å) as a function of temperature, compared to b (0.037 Å) and c (0.033 Å) (Table 2).

Note that despite the isostructural topology of the silicates and the nonsilicates, the type and the orientation of the Jahn-Teller distortion are different. This difference reinforces the statement of Hoffmann et al. (1997) that
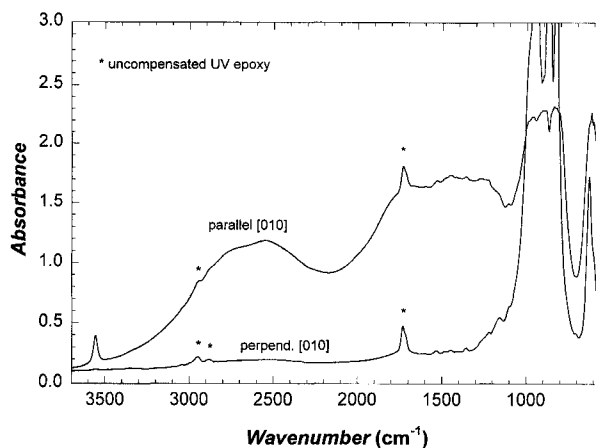
the same mode of octahedral chain connection does not imply the same type of Jahn-Teller distortion.

The H atom position

A direct consequence of the Jahn-Teller distortion of the $Mn^{3+}O_6$ octahedron in mozartite is the position of the H atom. McNear et al. (1976) refined the H position in vuagnatite close to O5 with a strong hydrogen bond to O2. Unlike in vuagnatite, where O5 possesses a valence sum of 1.57 v.u., the relatively short, Jahn-Teller compressed M-O5 distances in mozartite increase the valence sum of O5 (bonded to two M cations and one Ca atom) to 1.867 v.u., thus O5 in mozartite is not privileged to form an OH group. In general, the OH group in minerals of the adelite group (Basso et al. 1989; Cesbron et al. 1987) is part of the octahedron (at O5). In the original structure description of mozartite (Basso et al. 1993) the H position close to O5, attached to the octahedron, was extracted from difference-Fourier maps but not refined. However, as stated above, this proton position in mozartite seems fairly unlikely considering the O5 valence sum of 1.867 v.u. (without accounting for H). From this point of view, the valence sums of O2 (bonded to two Ca atoms and one Si atom) may be compared for vuagnatite and mozartite. All bonds to O2 in mozartite [1.647(2) Å to Si; 2.469(2) Å to Ca; 2.626(2) Å to Ca] are significantly longer than corresponding distances in vuagnatite [1.615(2) Å to Si; 2.328(2) Å to Ca; 2.482(2) Å to Ca]. Thus the O2 valence sum decreases from 1.589 v.u. (vuagnatite) to 1.365 v.u. (mozartite). Therefore, the OH group in mozartite is at O2 (the apex of the tetrahedron) and is hydrogen bonded to O5, whereas in vuagnatite the OH group is at O5 and is hydrogen bonded to O2.

The performed network calculations confirm this result. A comparison between the two models shows that predicted bond lengths for an O2-H $\cdots$ O5 model agree very well with the observed geometry, both the lattice-stress induced distortion around Mn^{3+} (neglecting the Jahn-Teller effect) as well as the H-induced distortion of

the Si tetrahedron. The O5-H $\cdots$ O2 model (Basso et al. 1993), on the other hand, leads to significant discrepancies. This model no longer predicts O5-Mn-O5 to be the shortest octahedral diagonal, and more importantly the bond lengths of the $SiO_3(O \cdots H)$ tetrahedron are not reproduced properly. The longest tetrahedral bond, Si-O2 [1.662 Å according to Basso et al. (1993) and 1.647 Å in this study at 300 K], is predicted to be the shortest (1.593 Å).

The $SiO_3(OH)$ tetrahedron

The tetrahedron in mozartite is quite regular with O-Si-O angles between 101.2 and 115.2° (at 100 K), and the largest and smallest angles are associated with O2, the OH group. Distances between Si and O1, O3, and O4 are about 1.635 Å and very similar between 100 and 300 K. The distance to the OH group Si-O2 (1.650 Å) is the longest within the tetrahedron. The displacement parameters of the tetrahedral atoms (Table 5) reflect the following trends: $<\Delta U(\text{par})>$ ($\cong$ 0.0005 Å^2) values are temperature independent, which is characteristic of SiO_4 rigid-body behavior (Kunz and Armbruster 1990); $<\Delta U(\text{perp})>$, without considering O2, increases with temperature, which is characteristic of a librational motion of the entire tetrahedron. The $\Delta U(\text{perp})$ values of the Si-O2 bond are analyzed separately because O2 is only weakly fixed by soft bonds to Ca and the hydrogen bond between O2-H $\cdots$ O5. The $\Delta U(\text{perp})$ value of O2 shows a much steeper slope with temperature than $\Delta U(\text{perp})$ of the other tetrahedral O atoms. Thus in addition to the tetrahedral rigid-body libration, the Si-O2 vector undergoes an independent librational motion that weakens the O2-H $\cdots$ O5 hydrogen bond. This weakening can also be seen in the temperature dependence of the O2 $\cdots$ O5 separation, which increases from 2.480 Å at 100 K to 2.517 Å at 500 K.

FTIR spectroscopy

Polarized single-crystal IR spectra of mozartite at room temperature show a strong, broad absorption parallel to b in the region between 3300 and 400 cm^{-1}. Because this absorption is superimposed on lattice and silicate modes (and their overtones around 2800–2500 cm^{-1}) the center of absorption can only roughly be estimated to lie between 1700 and 1300 cm^{-1}. At 84 K the band appears to be slightly increased and sharper, with its center shifted toward the region around 1300–1400 cm^{-1}. The polarized IR absorption spectra perpendicular to the b direction do not show this broad band.

Different arguments favor an assignment of this broad band to the stretching mode of the hydroxide group in mozartite. First, the exclusive polarization parallel to b is in agreement with the orientation of the O-H vector in the mozartite structure. Second, according to the frequency-bond length correlation diagram of Novak (1974) the frequency of this band is in good agreement with the observed O-H $\cdots$ O distance in mozartite. According to Novak (1974), the range 1300–1700 cm^{-1} is correlated to

2.48–2.52 Å between O donor and acceptor atoms. The shift toward lower band energies upon cooling is in agreement with the slight shortening of the hydrogen bond at 100 K. And third, the band shape of the broad band, which is superimposed on other absorptions, is typical for such strong hydrogen bonds (Novak 1974).

Finally, the weak but sharp absorption band in the b spectrum at 3557 cm^{-1} must be mentioned. This band is assigned to an almost free OH group (according to its frequency) that is aligned approximately parallel to the b axis. The slight shift toward higher frequencies upon cooling is in agreement with only weak or no hydrogen bonding interaction (Lutz 1995). However, the low intensity of this band indicates that this OH group is probably due to structural defects rather than due to a stoichiometric component of the mozartite structure.

REFERENCES CITED

Armbruster, T. and Geiger, C.A. (1993) Andradite crystal chemistry, dynamic X-site disorder and structural strain in silicate garnets. European Journal of Mineralogy, 5, 57–71.

Baerlocher, Ch., Hepp, A., and Meier, W.M. (1977) DLS-76, a program for the simulation of crystal structures by geometric refinement, EidgenössischeTechnische Hochschule Zürich, Switzerland.

Bartelmehs, K.L., Downs, R.T., Gibbs, G.V., Boisen, M.B.Jr., and Birch, J.B. (1995) Tetrahedral rigid-body motion in silicates. American Mineralogist, 80, 680–690.

Basso, R., Lucchetti, G., and Zefiro, L. (1993) Mozartite, CaMn(OH)SiO$_4$, a new mineral species from the Cerchiara mine, Northern Apennines, Italy. Canadian Mineralogist, 31, 331–336.

Basso, R., Palenzona, A., and Zefiro, L. (1989) Crystal structure refinement of a Sr-bearing term related to copper vanadates and arsenates of adelite and descloizite groups. Neues Jahrbuch der Mineralogie, Monatshefte, 1989, 300–308.

Brese, N.E. and O'Keeffe, M. (1991) Bond valence parameters for solids. Acta Crystallographica, B47, 192–197.

Brown, I.D. (1976) On the geometry of O-H...O hydrogen bonds. Acta Crystallographica, A32, 24–31.

———(1989) Using chemical bonds to analyze data retrieved from the inorganic crystal structure database. Journal of Chemical Information and Computer Science, 29, 266–271.

———(1992) Chemical and steric constraints in inorganic solids. Acta Crystallographica, B48, 553–572.

Brown, I.D. and Altermatt, D. (1985) Bond-valence parameters obtained from a systematic analysis of the Inorganic Crystal Structure Database. Acta Crystallographica, B41, 244–247.

Cesbron, F.P., Ginderov, D., Giraud, R., Pelisson, P., and Pilard, F. (1987) La nickelaustinite Ca(Ni,Zn)(AsO$_4$)(OH): nouvelle espèce minérale du district cobalto-nickelifère de Bou-Azzer, Maroc. Canadian Mineralogist, 25, 401–407.

Chandrasekhar, K. and Bürgi, H.B. (1984) Dynamic processes in crystals examined through difference vibrational parameters ΔU: the low-

spin–high-spin transition in tris(dithiocarbamato)iron(III) complexes. Acta Crystallographica, B40, 387–397.

Dunitz, J.D., Schomaker, V., and Trueblood, K.N. (1988) Interpretation of atomic displacement parameters from diffraction studies of crystals. Journal of Physical Chemistry, 92, 856–867.

Enraf-Nonius (1983) Structure determination package SDP, Enraf Nonius, Delft.

Gazo, J., Bersuker, I.B., Garaj, J., Kabesova, M., Kohout, J., Langfelderova, H., Melnik, M., Serator, M., and Valach, F. (1976) Plasticity of the coordination sphere of copper(II) complexes, its manifestation and causes. Coordination Chemistry Reviews, 1976 (19), 253–299.

Giuseppetti, G. and Tadini, C. (1988) The crystal structure of austinite, $CaZn(AsO_4)(OH)$, from Kamareza, Laurion, Greece. Neues Jahrbuch für Mineralogie, Monatshefte, 1988, 159–166.

Gottardi, G. (1967) Structural features of some group-silicates with chains of octahedra. Tschermaks mineralogische und petrographische Mitteilungen, 12, 129–139.

Hoffmann, C., Armbruster, T., and Kunz, M. (1997) Structure refinement of (001) disordered gaudefroyite $Ca_4Mn_3^{3+}[(BO_3)(CO_3)O_3]$: Jahn-Teller-distortion in edge-sharing chains of $Mn^{3+}O_6$ octahedra. European Journal of Mineralogy, 9, 7–19.

Hitchman, M.J. (1994) The influence of vibronic coupling on the spectroscopic properties and stereochemistry of simple 4- and 6-coordinate copper(II) complexes. Comments on Inorganic Chemistry, 15, 197–254.

Kunz, M. and Armbruster, T. (1990) Different displacement parameters in alkali feldspars: effects of (Si, Al) order-disorder. American Mineralogist, 75, 141–149.

Kunz, M. and Brown, I.D. (1995) Out-of-center distortions around octahedrally coordinated d^0 transition metals. Journal of Solid State Chemistry, 115, 395–406.

Lutz, H.D. (1995) Hydroxide ions in condensed materials—Correlation of spectroscopic and structural data. Structure and Bonding, 82, 85–103.

McNear, E., Vincent, M.G., and Parthé, E. (1976) The crystal structure of vuagnatite. American Mineralogist, 61, 831–838.

Novak, A. (1974) Hydrogen bonding in solids. Correlation of spectroscopic and structural data. Structure and Bonding, 18, 177–216.

Qurashi, M.M. and Barnes, W.H. (1963) The structure of the minerals of the descloizite and adelite groups. IV. Descloizite and conichalcite (part 2). The structure of conichalcite. Canadian Mineralogist, 7, 561–577.

Riley, M.J., Hitchman, M.A., and Mohammed, A.W. (1987) Interpretation of the temperature dependent g values of the $Cu(H_2O)_6^{2+}$ ion in several host lattices using a dynamic vibronic coupling model. Journal of Chemical Physics, 87, 3766–3778.

Shannon, R.D. (1976) Revised effective radii and systematic studies of interatomic distances in halides and chalcogenides. Acta Crystallographica, A32, 751–767.

Shen, J. and Moore, P.B. (1982) Törnebohmite, $RE_2Al(OH)(SiO_4)_2$: crystal structure and genealogy of RE (III)Si(IV) ↔ Ca(II)P(V) isomorphisms. American Mineralogist, 67, 1021–1028.

Siemens (1990) SHELXTL PC, 4.1, Siemens analytical X-ray instruments, Inc., Madison, WI.